

This is the peer reviewed version of the following article:

Size-segregated aerosol in a hot-spot pollution urban area: Chemical composition and three-way source apportionment / Bernardoni, V.; Elser, M.; Valli, G.; Valentini, S.; Bigi, Alessandro; Fermo, P.; Piazzalunga, A.; Vecchi, R.. - In: ENVIRONMENTAL POLLUTION. - ISSN 0269-7491. - 231:Pt 1(2017), pp. 601-611. [10.1016/j.envpol.2017.08.040]

*Terms of use:*

The terms and conditions for the reuse of this version of the manuscript are specified in the publishing policy. For all terms of use and more information see the publisher's website.

06/10/2024 14:23

(Article begins on next page)

## Manuscript Details

<b>Manuscript number</b>	ENVPOL_2017_2524
<b>Title</b>	Size-segregated aerosol in a hot-spot pollution urban area: Chemical composition and three-way source apportionment
<b>Article type</b>	Research Paper

### Abstract

In this work, a comprehensive characterisation and source apportionment of size-segregated aerosol collected using a multistage cascade impactor was performed. The samples were collected during wintertime in Milan (Italy), which is located in the Po Valley, one of the main pollution hot-spot areas in Europe. For every sampling, size-segregated mass concentration, elemental and ionic composition, and levoglucosan concentration were determined. Size-segregated data were inverted using the program MICRON to identify and quantify modal contributions of all the measured components. The detailed chemical characterisation allowed the application of a three-way (3-D) receptor model (implemented using Multilinear Engine) for size-segregated source apportionment and chemical profiles identification. It is noteworthy that - as far as we know - this is the first time that three-way source apportionment is attempted using data of aerosol collected using traditional cascade impactors. Seven factors were identified: wood burning, industry, resuspended dust, regional aerosol, construction works, traffic 1, and traffic 2. Further insights into size-segregated factor profiles suggested that the traffic 1 factor can be associated to diesel vehicles and traffic 2 to gasoline vehicles. The regional aerosol factor resulted to be the main contributor (nearly 50%) to the droplet mode (accumulation sub-mode with modal diameter in the range 0.5-1  $\mu\text{m}$ ), whereas the overall contribution from the two factors related to traffic was the most important one in the other size modes (34-41%). The results showed that applying a 3-D receptor model to size-segregated samples allows identifying factors of local and regional origin while receptor modelling on integrated PM fractions usually singles out factors characterised by primary (e.g. industry, traffic, soil dust) and secondary (e.g. ammonium sulphate and nitrate) origin. Furthermore, the results suggested that the information on size-segregated chemical composition in different size classes was exploited by the model to relate primary emissions to rapidly-formed secondary compounds.

<b>Keywords</b>	Multistage cascade impactor; aerosol size distribution; size-segregated chemical composition; three-way source apportionment; gasoline vehicles; diesel vehicles
<b>Corresponding Author</b>	Roberta Vecchi
<b>Order of Authors</b>	Vera Bernardoni, Miriam Elser, Gianluigi Valli, Sara Valentini, Alessandro Bigi, PAOLA FERMO, Andrea Piazzalunga, Roberta Vecchi
<b>Suggested reviewers</b>	Peter Molnár, Fulvio Amato, claudio Belis, Wioletta Rogula-Kozłowska, Imre SALMA

1 **Size-segregated aerosol in a hot-spot pollution urban area: Chemical composition and three-**  
2 **way source apportionment**

3 V. Bernardoni<sup>1</sup>, M. Elser<sup>1,#</sup>, G. Valli<sup>1</sup>, S. Valentini<sup>1</sup>, A. Bigi<sup>2</sup>, P. Fermo<sup>3</sup>, A. Piazzalunga<sup>3,§</sup>, R.  
4 Vecchi<sup>1,\*</sup>

5 <sup>1</sup>Dipartimento di Fisica, Università degli Studi di Milano and INFN-Milan, Milan, Italy

6 <sup>2</sup>Dipartimento di Ingegneria "Enzo Ferrari", Università degli Studi di Modena e Reggio Emilia,  
7 Modena, Italy

8 <sup>3</sup>Dipartimento di Chimica, Università degli Studi di Milano, Milan, Italy

9 <sup>#</sup>now at: Swiss Federal Laboratories for Materials Science and Technology, Empa, Dübendorf,  
10 Switzerland

11 <sup>§</sup>now at: Water & Life Lab, Entratico (BG), Italy

12

13 \*Corresponding Author:

14 Prof. Roberta Vecchi

15 Dipartimento di Fisica

16 Università degli Studi di Milano

17 Via Celoria 16

18 20133 Milan

19 Italy

20 tel: +39 02 50317498

21 email: roberta.vecchi@unimi.it

22

23 **Abstract**

24 In this work, a comprehensive characterisation and source apportionment of size-segregated aerosol  
25 collected using a multistage cascade impactor was performed. The samples were collected during  
26 wintertime in Milan (Italy), which is located in the Po Valley, one of the main pollution hot-spot  
27 areas in Europe.

28 For every sampling, size-segregated mass concentration, elemental and ionic composition, and  
29 levoglucosan concentration were determined. Size-segregated data were inverted using the program  
30 MICRON to identify and quantify modal contributions of all the measured components.

31 The detailed chemical characterisation allowed the application of a three-way (3-D) receptor model  
32 (implemented using Multilinear Engine) for size-segregated source apportionment and chemical  
33 profiles identification. It is noteworthy that - as far as we know - this is the first time that three-way  
34 source apportionment is attempted using data of aerosol collected using traditional cascade  
35 impactors. Seven factors were identified: wood burning, industry, resuspended dust, regional

36 aerosol, construction works, traffic 1, and traffic 2. Further insights into size-segregated factor  
37 profiles suggested that the traffic 1 factor can be associated to diesel vehicles and traffic 2 to  
38 gasoline vehicles. The regional aerosol factor resulted to be the main contributor (nearly 50%) to  
39 the droplet mode (accumulation sub-mode with modal diameter in the range 0.5-1  $\mu\text{m}$ ), whereas the  
40 overall contribution from the two factors related to traffic was the most important one in the other  
41 size modes (34-41%).

42 The results showed that applying a 3-D receptor model to size-segregated samples allows  
43 identifying factors of local and regional origin while receptor modelling on integrated PM fractions  
44 usually singles out factors characterised by primary (e.g. industry, traffic, soil dust) and secondary  
45 (e.g. ammonium sulphate and nitrate) origin. Furthermore, the results suggested that the information  
46 on size-segregated chemical composition in different size classes was exploited by the model to  
47 relate primary emissions to rapidly-formed secondary compounds.

48

49 *Capsule:* detailed chemical characterisation of samples collected by multistage cascade impactor  
50 was performed. Application of three-way receptor model allowed obtaining size-segregated source  
51 apportionment.

52

53 **Keywords:** Multistage cascade impactor; aerosol size distribution; size-segregated chemical  
54 composition; three-way source apportionment; gasoline vehicles; diesel vehicles

55

## 56 **1. Introduction**

57 Atmospheric aerosol is a complex mixture of solid and liquid particles suspended in the  
58 atmosphere. Atmospheric aerosol has impacts at local scale on health (e.g. Pope and Dockery,  
59 2006), visibility (e.g. Watson, 2002), cultural heritage damage (e.g. Bonazza et al., 2005) and at  
60 global scale on the Earth radiation balance (IPCC, 2013). The main parameters determining the  
61 aerosol effects are particle sizes and chemical properties, which depend on source emissions and  
62 following transformations/reactions in atmosphere (Pöschl, 2005). As examples, size-segregated  
63 information can be used to gain further insights into aerosol effects on health (Heal et al., 2012) and  
64 can be exploited in perspective to improve Earth radiative transfer models.

65 Atmospheric aerosol can be separated in several size-ranges and collected for subsequent analysis  
66 using multistage cascade impactors. Measurement techniques for the characterisation of different  
67 components of size-segregated aerosol have been described in the literature (e.g. Maenhaut et al.,  
68 1999 for elemental analysis by Particle-Induced X-ray emission; Viidanoja et al., 2002 for organic  
69 and elemental carbon analysis). To provide complete chemical characterisation, sampling on  
70 different filter media is mandatory (e.g. Maenhaut et al., 2002; Rogula-Kozłowska, 2016; Salma et

71 al., 2005). Nevertheless, sampling using cascade impactors is not straightforward, mainly due to the  
72 number of samples to deal with. Thus, it can be worthy developing non-destructive, traditional  
73 techniques (e.g. ED-XRF) to provide a relatively wide chemical characterisation on the same  
74 sample with no need of unconventional laboratory devices (e.g. accelerators).

75 Information on aerosol sources can be obtained from physical-chemical characterisation of aerosol  
76 collected in ambient air e.g. using multivariate receptor models (Hopke, 2016; Viana et al., 2008;  
77 and therein cited literature), which allow to retrieve aerosol source contributions, chemical profiles,  
78 and temporal trends. Three-way (3-D) source apportionment models (Harshman and Lundy, 1994;  
79 Tucker, 1966) can be applied to size- and time-resolved aerosol samples to obtain information on  
80 size-segregated source profiles and contributions. Nevertheless, in spite of the importance of  
81 exploiting information on size-segregated aerosol composition for source apportionment purposes,  
82 studies concerning a comprehensive characterisation of aerosol segregated in more than two size  
83 classes coupled to 3-D source apportionment are nearly absent in the literature. Few examples are  
84 applications to data collected using a high-resolution time-of-flight mass spectrometer - HR-ToF-  
85 MS (Ulbrich et al., 2012) or drum impactors (Li et al., 2013; Peré-Trepat et al., 2007). Nevertheless,  
86 the high cost and complex operation of the HR-ToF-AMS and the need of accelerator facilities for  
87 the elemental analysis of drum impactor samples (Bukowiecki et al., 2005; Cahill, 1996) strongly  
88 limit the spatial and temporal applicability of these techniques.

89 In this work, a comprehensive characterisation of size-segregated aerosol collected using a  
90 multistage cascade impactor was performed quantifying mass by gravimetry, elements by ED-XRF,  
91 main inorganic ions and levoglucosan by liquid chromatographic techniques. The detailed size-  
92 segregated characterisation allowed the determination of mass and chemical components size  
93 distribution at a heavily polluted area (Milan, Italy). Furthermore, a 3-D receptor model  
94 (implemented using Multilinear Engine) was applied to obtain size-segregated source profiles and  
95 apportionment from samples collected using traditional multistage cascade impactors. As far as we  
96 know, this is the first time that 3-D source apportionment is attempted on this kind of data.

97

## 98 **2. Materials and Methods**

### 99 **2.1 Sampling**

100 Aerosol was sampled using a multistage cascade impactor collecting particles in 12-stages with  
101 nominal cut-off diameter in the range 45 nm - 8.5  $\mu\text{m}$  (SDI, Dekati - more details in Bernardoni et  
102 al., 2011a). Samples were collected on coated polycarbonate substrates to avoid particle bouncing  
103 among impaction stages. Coating was performed using DS-515 spray by Dekati. Upstream the  
104 impactor, a PM10 EPA-equivalent inlet was used. It is noteworthy to recall that EPA inlets are  
105 designed to perform a 10  $\mu\text{m}$  cut-off at 16.67 l/min. Considering the SDI flow-rate (11.12 l/min),

106 the expected size-cut of the inlet in this work was calculated to be 12.2  $\mu\text{m}$ .  
107 Samplings were performed at an urban background site in the University Campus in the period  
108 January-March 2011. Fourteen samplings were performed with a time resolution in the range 24-48  
109 h, for a total of 168 polycarbonate foils available for the analysis.  
110 During the sampling period, median temperature was 7.4°C (range: -2.7°C to 20.0°C, except for the  
111 last three samplings when temperatures up to 24°C were reached). Average wind speed was 0.72  
112 m/s. Wind speed higher than 4 m/s were occasionally registered during a Foehn event (15<sup>th</sup>  
113 February). Precipitations occurred during 1 sampling only, with a rate lower than 2 mm/h. The  
114 integral precipitation during that sampling was 6.4 mm.

115

## 116 **2.2 Laboratory analyses**

117 All the substrates were weighed before and after the sampling using an analytical microbalance  
118 (precision 1  $\mu\text{g}$ ) in an air-conditioned weighing room ( $T = 20 \pm 1^\circ\text{C}$  and R.H. =  $50 \pm 5\%$ ). Before  
119 weighing, filters were placed on open but dust-protected sieve-trays for 48 hours in the weighing  
120 room for conditioning. The weighing protocol is described in Vecchi et al. (2004). Calibration  
121 procedures checked the microbalance performance.

122 Elemental composition (S, Cl, K, Ca, Ti, V, Cr, Mn, Fe, Ni, Cu, Zn, Br, Pb) was determined on all  
123 samples using an Energy-Dispersive X-Ray Fluorescence instrument (ED-2000, Oxford) suitably  
124 set up for the analysis of samples collected using multistage cascade impactors (details in  
125 Bernardoni et al., 2011a). Minimum detection limits were in the range 1-20 ng/sample, depending  
126 on the considered element (except for S and Cl: 140 and 89 ng/sample, respectively), corresponding  
127 to about 0.1-8.9 ng/m<sup>3</sup> when considering sampling volumes. Uncertainties were estimated in the  
128 range 7-15% for most elements and samples.

129 After ED-XRF analysis, which is fully not destructive, all the samples were water extracted for the  
130 determination of the main inorganic ions ( $\text{SO}_4^-$ ,  $\text{NO}_3^-$ ,  $\text{NH}_4^+$ ,  $\text{K}^+$ ) and levoglucosan. Extraction of  
131 each sample was performed using 30  $\mu\text{l}$  methanol and 3 ml MilliQ water, sonicating for 1 h. The  
132 main inorganic ions were determined by ion chromatography (details in Piazzalunga et al., 2013).  
133 Minimum detection limits were 25 ng/sample for ammonium (0.7-1.6 ng/m<sup>3</sup> depending on sampling  
134 volume), 100 ng/sample for sulphate and nitrate (3.2-7.3 ng/m<sup>3</sup>), and 170 ng/sample for potassium  
135 (5.4-12.3 ng/m<sup>3</sup>). Uncertainties were about 10%. Levoglucosan measurements were performed by  
136 high-performance liquid chromatography coupled to pulsed-amperometric detection (HPAEC–  
137 PAD) (details in Piazzalunga et al., 2010). Minimum detection limit was 11 ng/sample (0.4-0.8  
138 ng/m<sup>3</sup>) and uncertainties were about 10%.

139

## 140 **2.3 Modes retrieval by the program MICRON.**

141 For each measured component, size segregated concentration measured by multistage impactors is  
 142 usually represented as histogram (see Figure 1a). Each bar of the histogram is related to the  
 143 characteristics of the considered impactor stage and of the collected aerosol as follows: the bar  
 144 width (represented in log-scale) extends from the cut-off of considered stage and the cut-off of the  
 145 previous one (i.e. the adjacent stage with higher cut-off); the bar height represents  $\Delta m / \Delta \log(d_p)$   
 146 where  $\Delta m$  is the component mass measured on the considered stage and  $\Delta \log(d_p)$  is the difference  
 147 between the logarithms of the cut-off diameters of the previous and considered stages. When a  
 148 continuous distribution is of interest,  $dm/d(\log(d_p))$  as a function of  $d_p$  are represented (note that  
 149 when  $\log(d_p)$  is used, it has to be intended as  $\log(d_p/d_{p0})$ , where  $d_{p0}=1\mu m$ , for details see Seinfeld  
 150 and Pandis, 1998). Nevertheless, a more accurate representation of the original size distribution has  
 151 to take into account real cut-off curves of the impactor. To this aim, the inversion program  
 152 MICRON (Wolfenbarger and Seinfeld, 1990) was used to retrieve the original size distribution of  
 153 the different chemical components for each sampling (see Figure 1b). The inversion is based on a  
 154 constrained regularisation algorithm. Model inputs are the mass/species concentrations collected on  
 155 each impaction stage, which are redistributed considering the actual collection efficiency of the SDI  
 156 impactor (Hillamo, 1994) and the uncertainties on input data. Each inverted  $dm/d(\log(d_p))$   
 157 distribution is then fitted with log-normal functions (see Figure 1c) to retrieve the geometric mean  
 158 aerodynamic diameter (GMAD), and the different contributions of the modes (Maenhaut et al.,  
 159 1996).

160

## 161 **2.4 Source apportionment**

162 Source apportionment was performed using a vector-matrix decomposition, inspired to the Tucker1  
 163 model (Tucker, 1966). In this model, each element  $x_{i,j,k}$  of the 3-D input matrix representing the M  
 164 species of the aerosol collected in N stages of a cascade impactor during R samplings is factorised

165 in S (unknown) factors as follows:  $x_{i,j,k} = \sum_{p=1}^S b_{i,j,p} a_{p,k} + \epsilon_{i,j,k}$ , where  $\epsilon_{i,j,k}$  is the difference between the

166 measured and the modelled concentrations. Different meanings can be attributed to the factorising  
 167 terms (Ulbrich et al., 2012). In our decomposition,  $b_{i,j,p}$  ( $1 \leq i \leq N$ ,  $1 \leq j \leq M$ ,  $1 \leq p \leq S$ ) was an element  
 168 of an  $N \times M \times S$  array, where each  $N \times M$  layer represents the size-segregated p-th factor profile and  
 169  $a_{p,k}$  ( $1 \leq k \leq R$ ) represents the contribution of the p-th factor to the k-th sampling.

170 The model was implemented using Multilinear Engine - ME-2 (Paatero, 1999) and is based on the

171 minimisation of the object function  $Q = \sum_i \sum_j \sum_k \frac{\epsilon_{i,j,k}^2}{\sigma_{i,j,k}^2}$ , where  $\sigma_{i,j,k}$  is the uncertainty associated to

172 each  $x_{i,j,k}$ . The function Q previously reported represents the main equation of the model. Further  
 173 constraints can be applied by adding other terms (auxiliary equations). The conjugate gradient

174 algorithm is used to compute the solution. Non-negativity constraints are implemented by using the  
175 well-known technique of pre-conditioning in opposite way for slowing down changes of variables  
176 that are about to become negative. Factor scaling indeterminacy can be removed including a priori  
177 information on factor matrices. In our case, normalisation was carried out as follows:  $\sum_k a_{p,k} = 1$  for  
178 each factor p.  
179 The model was run using strong variables (Paatero 2015). This excluded Cr and Ni. S and  $\text{SO}_4^-$   
180 showed very good correlation and correct stoichiometric ratio.  $\text{SO}_4^-$  was chosen because of the  
181 higher associated explained mass. The choice between  $\text{K}^+$  and K was performed considering that  
182 they were very well correlated for  $d \leq 2.70 \mu\text{m}$  but K provided significant contribution also in larger  
183 size fractions (due to insoluble K related e.g. to potassium oxides in crustal material). Thus, K was  
184 chosen as input. Cl resulted with no other tracers in a single factor accounting for few mass thus  
185 preventing physical interpretation. Summarising, twelve variables were chosen as input data: K, Ca,  
186 Ti, Mn, Fe, Cu, Zn, levoglucosan,  $\text{SO}_4^-$ ,  $\text{NO}_3^-$ ,  $\text{NH}_4^+$ , and mass. It is noteworthy that carbonaceous  
187 material was not measured so that unexplained mass (i.e. the difference between the mass and the  
188 detected species) ranged from 34% to >95% depending on the sample. Generally, the highest  
189 unexplained mass was registered in very small size classes: this was consistent with the small size  
190 expected for carbonaceous particles emitted from combustion processes.

191 Data and uncertainties were treated following Polissar et al. (1998). In our case,  $\sigma_{i,j,k}$  was the  
192 analytical uncertainty associated to the chemical species. Exception was the uncertainty associated  
193 to the mass as it was increased to 4-times the mass value. Indeed, mass was considered as “total  
194 variable”, i.e. it was used to determine factor scaling and for source contribution quantification.  
195 Total variable should not have strong influence on the solution, thus it should be always down-  
196 weighed (EPA, 2014).

197 Species were measured in 168 samples. Data were arranged into a 3-D matrix representing 12 size  
198 classes  $\times$  12 species  $\times$  14 samplings. Missing data were identified as -999 and were automatically  
199 excluded by the program in the computation of the Q function. Due to the unknown number of  
200 factors, solutions for different numbers of factors were explored to identify the best solution.  
201 Multiple minima are a crucial issue in 3-D models. Thus, the global minimum and a few of the  
202 deepest local minima were explored (Paatero, 2000).

203

### 204 **3. Results and discussion**

#### 205 ***3.1 Mass and chemical components size distribution***

206 All the size-segregated data concerning mass and chemical components for all the samplings were  
207 inverted using the program MICRON as explained in paragraph 2.3.



208 For what concerns aerosol mass, two different types of mass size distributions were detected in the  
209 measured data (see Figure 2). They mainly differed in the absence (type 1) or presence (type 2) of a  
210 detectable Aitken mode at about 100 nm. The presence of the Aitken mode has probably to be  
211 ascribed to samples impacted by fresh and local emissions and its absence to a more aged aerosol.  
212 Some literature works argued the possibility of vapour condensation during low-pressure impactor  
213 sampling due to expansion cooling. Nevertheless, Raabe et al. (1988) did not find it as an issue  
214 considering that the lower temperature is reached instantaneously and maintained only for short  
215 time (of the order of  $\mu\text{s}$ ). When present, the Aitken mode accounted on average for 9% of the  
216 measured mass.

217 For  $d > 100$  nm, the mass size distribution showed the accumulation mode separated into two sub-  
218 modes (condensation mode and droplet mode, e.g. see Seinfeld and Pandis, 1998) and the coarse  
219 mode. GMADs for condensation, droplet, and coarse modes were 0.28  $\mu\text{m}$ , 0.72  $\mu\text{m}$ , 4.1  $\mu\text{m}$ ,  
220 respectively, for mass size distribution type 1; for mass size distribution type 2, GMADs for the  
221 three modes were 0.29  $\mu\text{m}$ , 0.71  $\mu\text{m}$ , 3.7  $\mu\text{m}$ . Mode GMADs were very similar to previously  
222 literature findings (e.g. Cabada et al., 2004; Salma et al., 2005). Whether no significant differences  
223 in mode GMADs were present between the two size distribution types, the relative contribution of  
224 condensation and droplet modes was different: indeed, in mass size distribution type 1 the  
225 contribution of the droplet mode was significantly higher than in the other case. This observation  
226 and the absence of the Aitken mode evidenced the role of aging processes leading to the increase of  
227 particle sizes.

228 Modal distributions for all the measured chemical components were retrieved. Condensation,  
229 accumulation, and coarse modes, as well as very large particles were detected for most species,  
230 whereas Aitken nuclei mode was detected for levoglucosan,  $\text{NO}_3^-$ ,  $\text{SO}_4^{2-}$ , and  $\text{K}^+$ . Results concerning  
231 these modes GMADs, relative mass concentration (RMC) (when modes were present), and the  
232 relative number of cases in which modes occurred were summarised in Table 1. Furthermore, an  
233 "intermediate mode" (not shown in Table 1) with  $0.9 \mu\text{m} \leq \text{GMAD} \leq 1.2 \mu\text{m}$  was detected in more  
234 than 85% cases for Ca, Ti, Fe, Cu, and in 36% cases for Ni. When present, the intermediate mode  
235 accounted for less than 25% of the total mass of the species. An intermediate mode was already  
236 found for Ca, Ti, and Fe at urban sites in the literature (Pakkanen et al., 2001; Salma et al., 2005),  
237 where coal combustion (not expected to impact the samples presented in this work), regional, and  
238 mineral aerosol related to road dust were mentioned as possible origin of the mode.

239 It is noteworthy that information on the size distribution of chemical components is very important  
240 e.g. to provide information useful for the assessment of aerosol health effects and to constrain  
241 inputs to Earth radiative transfer models.

242 In Figure 3a, the size distribution for secondary inorganic ions was shown. The droplet mode  
243 clearly prevailed on the condensation mode consistently with previous findings in the literature (e.g.  
244 Cabada et al., 2004), where gas-phase reactions were identified as responsible for the condensation  
245 mode formation. Heterogeneous formation, cloud processing, and growth of the condensation mode  
246 were indicated as processes leading to droplet mode increase. In addition, secondary inorganic ions  
247 presented the Aitken mode (4% relative contribution  $\text{SO}_4^-$ , 2% for  $\text{NH}_4^+$  and  $\text{NO}_3^-$ ). In the literature,  
248 direct emission of ultrafine inorganic ions (especially sulphate) were associated to combustion  
249 processes, as traffic (e.g. Robert et al., 2007) or wood/pellets burning (Ozgen et al., 2017).  
250 In Figure 3b, levoglucosan,  $\text{K}^+$ , and elemental K concentrations were shown. They are known  
251 tracers for wood burning (Kleeman et al., 1999; Simoneit et al., 1999; Viana et al., 2008). As  
252 expected, K gave a higher contribution than  $\text{K}^+$  because it referred to total (i.e. soluble plus  
253 insoluble) potassium concentration in atmospheric aerosol. Focusing on  $d_p < 1 \mu\text{m}$ , the major  
254 contribution for wood burning tracers was found in the accumulation sub-modes (as previously  
255 observed for secondary inorganic ions) but here the condensation mode dominated on the droplet  
256 mode, indicating different formation processes for particles containing these compounds compared  
257 to secondary inorganic ions. Furthermore, the presence of the Aitken mode suggested the likely  
258 impact of local (urban) emissions by wood/pellet burning. Indeed, recent literature works reported  
259 emissions of ultrafine particles containing levoglucosan by wood stoves and  $\text{K}^+$  by wood and pellet  
260 stoves (Ozgen et al., 2017). Ultrafine particles containing K and levoglucosan were identified also  
261 in ambient aerosol in relationship to residential wood burning (Corsini et al., 2017; Pirjola et al.,  
262 2017). For  $d_p > 1 \mu\text{m}$ , a much higher contribution from K than from  $\text{K}^+$  can be noticed indicating the  
263 contribution from insoluble potassium to be likely ascribed to crustal elements.

264 Figure 3b and Figure 3c represented markers wood burning and traffic sources (among the main  
265 sources identified in the Milan urban area in previous works – e.g. Bernardoni et al., 2011b). It is  
266 noteworthy that the size distributions for tracers of the two sources are completely different.  
267 Opposite, smaller differences are registered among species considered as tracers for the same  
268 source. Thus, 3-D receptor modelling was applied trying to exploit these differences to gain further  
269 details on emission sources.

270

### 271 **3.2 Receptor model results**

272 The Tucker 1 model was implemented in ME-2 as explained in paragraph 2.4. Receptor models are  
273 always affected by multiple solutions for what concerns the possible number of factors, scaling  
274 indeterminacy, local minima, and possibly rotations (not an issue in 3-D models). Some  
275 mathematical parameters were checked to identify a range of possible solution (expected vs.  
276 computed Q value, residuals distribution, and input values reconstruction) (e.g. Belis et al., 2014,

277 Paatero, 2000). All these parameters were evaluated and 5-8 factors were identified as best choices.  
278 Nevertheless, mathematics is not enough to determine the right number of factors and the  
279 possibility of data interpretation guides the definitive choice (Hopke, 2016; Paatero, 2000). Finally,  
280 the 7-factor solution was identified as the best one. The effects of different choices for factor  
281 number will be discussed at the end of the paragraph.

282 Factor profiles (total mass of each species normalised to the mass in the factor) and the percent of  
283 the species associated to each factor, as well as the mass size distribution of the factors were  
284 represented in Figure 4. The mass size distribution was represented both using histogram  
285 representation of the ME-2 output and mode representation obtained from data inversion and modes  
286 retrieval. In this way, it was possible gaining information on the mass modes GMADs and modes  
287 relative contribution to each factor (Table 2). Detailed size-segregated profiles were reported in  
288 Figure 5 with histogram representation of the size-segregated relative contribution of the species to  
289 the identified factors. In Figure 5, normalisation was carried out to the total average concentration  
290 of each species (analogous to percent species for size-segregated representation). Results given in  
291 Figure 4, Figure 5, and Table 2 were the bases for factor identification, as explained in the  
292 following. Mode-segregated source apportionment for the whole campaign was summarised in  
293 Figure 6.

294 The factor identified as "wood burning" was an important contributor to levoglucosan (37%) and at  
295 a lesser extent K, well-known tracers for this source, as well as for  $\text{SO}_4^-$  which was identified as  
296 directly emitted by both wood and pellets burning in the literature (e.g. Chandrasekaran et al., 2011;  
297 Iinuma et al., 2007). In Figure 5, the contribution of these species was detected also in the ultrafine  
298 range and their presence related to residential wood burning as mentioned before. Wood burning  
299 factor accounted for 13% of the measured mass. The mass was mainly concentrated in the  
300 condensation and droplet modes (96% in total), whereas the remaining 4% was in the Aitken mode.  
301 It should be noticed that the mass associated to this source has to be considered as accounting only  
302 for local (urban) wood burning contribution. Indeed, a regional contribution from wood burning  
303 should be also expected, as 36% of levoglucosan was associated to the regional aerosol factor (see  
304 later).

305 The factor identified as "industry" was the main contributor to Zn (35%), which has been identified  
306 as a marker for industrial emissions in previous works in the area (e.g. Bernardoni et al., 2011b;  
307 Marcazzan et al., 2003). The industry factor accounted on average for 8% of the measured mass.  
308 Most of the mass (58%) was contained in the condensation mode, this being among the main  
309 contributors to the mass measured in this mode (18%).

310 The factor identified as "resuspended dust" was an important contributor to Ti (27%) and Ca (21%)  
311 concentrations. Nevertheless, also components of anthropogenic origin were present and the factor

312 size distribution was characterised in nearly equal parts by fine (<1µm) and coarse particles (54%  
313 and 46%, respectively), thus suggesting that anthropogenic particles previously deposited in the  
314 ground are resuspended (e.g. by atmospheric agents) together with soil particles. This factor  
315 accounted on average for 13% of the measured mass, and it was one of the two main contributors to  
316 the coarse mode and very large particles (22%).

317 The factor identified as "regional aerosol" was the main single contributor to the measured  
318 concentration of nitrate (52%), sulphate (35%), and ammonium (49%). It can be assumed that these  
319 ions were entirely in the form of ammonium sulphate and ammonium nitrate as they were  
320 chemically balanced in the profile within 5%. As previously mentioned, this factor was responsible  
321 for high contributions to levoglucosan (36%) and K (24%) (tracers for wood burning), and to Fe  
322 (22%) and Cu (22%) (tracers for traffic) indicating that this factor was not only associated to  
323 secondary aerosol, but also to non-local (aged) contributions from primary sources. The regional  
324 aerosol factor was the main contributor to the total measured mass (31%) and to the droplet mode  
325 (50%), where 81% of the mass of the factor was found. No contribution from the regional aerosol  
326 factor was registered in the Aitken mode, mainly because particles in such mode are typically  
327 associated to fresh emissions and tend to coagulate towards the accumulation mode in short times.  
328 Particle aging further increases particle size, thus justifying the predominance of the droplet mode.  
329 Therefore, the absence of a contribution in the Aitken mode and the small contribution to the  
330 condensation mode (9%) were further confirmations of the regional origin of this factor.

331 The factor identified as "construction works" was the main single contributor to the Ca measured  
332 concentrations (31%). An association between Ca and construction works at the sampling site was  
333 already identified in previous works (Bernardoni et al., 2011b; Vecchi et al., 2009). Its average  
334 contribution to the measured mass was 7%. This factor contributed to 22% of the mass measured in  
335 the coarse and very large particle modes, where 49% of the mass associated to this factor was  
336 found. The coarse/very large particles contribution was ascribed to soil/construction material  
337 movement, whereas the contribution to the other modes was related mainly to construction  
338 machinery exhaust. It is noteworthy that construction works were locally carried out at the  
339 Department of Physics during the measurements period, thus justifying the high (32%) - and quite  
340 unexpected - contribution of construction works to the Aitken mode.

341 Two factors were associated to traffic sources and named "traffic 1" and "traffic 2". They showed  
342 very similar profiles, and they were both important contributors to Fe and Cu (overall 44%), Mn  
343 (overall 52%), and Ca (overall 32%). Fe and Cu are widely used as markers for traffic sources in  
344 source apportionment studies (Pant and Harrison, 2013; Viana et al., 2008). Mn and Ca are reported  
345 to have multiple sources, including traffic. As examples, Crilley et al. (2017) found important  
346 contribution of Mn from traffic in PM10, Amato et al. (2011) identified traffic as a major

347 responsible of Mn concentration in the coarse fraction; Ca is often found in traffic source profiles  
348 due to traffic-related resuspension or to the contribution of lubricating oils (Viana et al., 2008). It is  
349 noteworthy that the two factors did not represent "traffic exhaust" and "traffic non-exhaust"  
350 contributions, as the markers for non-exhaust emissions were present in both factors. As for size  
351 distributions, the mass of both factors was mainly concentrated in the two accumulation sub-modes  
352 (61% for traffic 1 and 69% for traffic 2). In both factors, 23-24% of the mass of the factor was  
353 concentrated in the coarse mode, but traffic 2 showed a further 12% mass contribution to very large  
354 particles.

355 The main differences between the two factor profiles were higher contributions from nitrate,  
356 ammonium, Mn, and Ti in traffic 2 and from Zn in traffic 1. Little information is present in the  
357 literature for what concerns elemental tracers for gasoline and diesel vehicles separately. Lin et al.  
358 (2005) evidenced that diesel emissions contributed more than gasoline to the Zn concentrations in  
359 ultrafine particles, whereas gasoline was a stronger emitter of ultrafine Mn and Cu. Wang and  
360 Hopke (2013) identified that a "Gasoline vehicle" factor by PMF by analysis on PM<sub>2.5</sub> samples  
361 collected in California was the main responsible of Mn concentration. Link et al. (2017) reported  
362 that vehicles equipped with three-way catalyst system (gasoline and liquid petroleum gasoline) have  
363 the potential for forming NH<sub>4</sub>NO<sub>3</sub> aerosol rapidly and in high yields in presence of OH radicals. In  
364 Figure 7, size-segregated distribution of Cu, Mn, and Zn in traffic 1 and traffic 2 factor profiles are  
365 shown in histogram representation. Normalisation was carried out setting to 1 the total mass of the  
366 single species in each profile. Log-scale was used also for the y-axis to allow better identification of  
367 the species contributions to the small-diameter ( $d \leq 155$  nm) cut-off stages (which were in any case  
368 a low fraction of the total mass of the species). It is noteworthy that Zn relative contribution in these  
369 stages was higher for traffic 1 (7.3% vs. 3.1% in traffic 2), whereas Cu (6.9%) and Mn (3.9%) were  
370 higher for the traffic 2 factor (1.0% Cu and 1.3% Mn in traffic1 factor profile). Furthermore, traffic  
371 2 showed 29% contribution from nitrate in the factor profiles (Figure 4).

372 All these pieces of information gave indication of a tentative assignment of traffic 1 to diesel  
373 vehicles and traffic 2 to gasoline vehicles contributions. A more detailed insight into these factors  
374 showed that traffic 1 factor accounted for 18% of the total measured mass and it was characterised  
375 by 83% relative unexplained mass (i.e. the difference between the mass and the sum of the species  
376 in the profile), whereas traffic 2 factor accounted for 10% of the total measured mass but the  
377 relative unexplained mass was only 51%. For diesel vehicles not equipped with anti-particulate  
378 filter, exhaust emissions are known to be at least one order of magnitude higher than gasoline  
379 exhaust emissions (e.g. May et al., 2014). It is noteworthy (e.g. Schauer et al., 2006) that the  
380 dominant component in exhaust emissions is carbonaceous material which was not detected in this  
381 work. Thus, the stronger exhaust contribution expected for diesel vehicles can justify the higher

382 unexplained mass detected in the traffic 1 factor. Considering that diesel vehicles include also  
383 heavy duty vehicles and that such vehicles have a higher potential of dust resuspension, assigning  
384 traffic 1 factor to diesel vehicles could justify also the presence of the very large particles in this  
385 factor and not in traffic 2.

386 Traffic 1 and traffic 2 overall contributions made traffic the most important source of particle mass  
387 in all modes but the droplet one, where the contribution from the regional aerosol factor was  
388 dominant. The overall contribution of the two traffic factors (28%) might appear higher than in past  
389 studies in the area (e.g. Bernardoni et al., 2011b where a contribution of 16% was reported during  
390 wintertime for PM<sub>10</sub> samples). Nevertheless, in Bernardoni et al. (2011b) most of secondary ions  
391 were accounted for in "secondary sulphate" and "secondary nitrates" factors: thus, the other factors  
392 (including traffic) included mainly primary contributions. Opposite, in this work the analysis on  
393 size-segregated samples showed secondary aerosol to be partially explained by specific urban  
394 sources. Amato et al. (2016) presented a source apportionment study on PM<sub>10</sub> data collected in  
395 Milan and found an overall 16% contribution for vehicle exhaust and non-exhaust and further 14%  
396 vehicle nitrate contribution from NO<sub>x</sub> emission inventory. Thus, the overall traffic contribution  
397 resulted very similar to the value obtained in the current work. All these results evidenced the  
398 ability of source apportionment applied to size-segregated samples to relate at least part of the  
399 secondary aerosol to specific sources.

400 Likely the information on chemical composition in different size classes was exploited by the model  
401 to relate primary emissions to rapidly-formed secondary compounds. In the regional aerosol factor  
402 only 7% of the total nitrate, 13% of sulphate, and 8% of ammonium were found in the four lowest  
403 size-classes. In most of other factors, different size distributions were found for secondary  
404 compounds. As examples, focusing on the four lowest size classes in the histograms in figure 5,  
405 42% and 41% of the total nitrate in each factor was found in this size range for industry and  
406 resuspended dust, respectively, whereas 19% and 17% was found for traffic 1 and wood burning,  
407 respectively.

408 For what concerns other possible solutions obtained running the ME-2 model, 6-factor solution was  
409 excluded because the contributions from "industry" and "construction works" factors mixed in a  
410 unique ("other anthropogenic") factor. Increasing to 8 factors, the additional factor could not be  
411 identified, as no chemical species tracer for known sources could be detected.

412 Finally, it should be noticed that the main features of the model output (i.e. separation of local vs.  
413 regional contributions; ability to identify separate factors associated to gasoline and diesel vehicles)  
414 are related to sample features (i.e. size-segregation and detailed chemical characterisation), thus  
415 they are not impacted by meteorological conditions. Nevertheless, the latter can affect the relative

416 contribution of the different sources and must be considered when sampling for monitoring  
417 purposes – out of the scope of this manuscript – is carried out.

418

#### 419 **4. Conclusions**

420 A study of size-segregated aerosol sampled by SDI multistage impactor was carried out during  
421 wintertime in the Milan urban area, which is located in the Po Valley, one of the major pollution  
422 hot-spots in Europe.

423 The samples were characterised for mass concentration, and elemental and inorganic ionic  
424 composition. Data inversion by the program MICRON and interpolation by log-normal functions  
425 allowed detecting and quantifying aerosol modes. Three or four modal mass size distributions were  
426 identified in the samples. In all cases, the highest fraction of the mass was found in the  
427 accumulation mode.

428 Similarities in size distributions of source tracers suggested the possibility to perform source  
429 apportionment. Three-way source apportionment was performed by implementing the Tucker 1  
430 model in ME-2. Seven factors were identified, namely wood burning, industry, resuspended dust,  
431 construction works, regional aerosol, traffic 1 and traffic 2. It is interesting to note that in previous  
432 studies performed in the area on PM<sub>10</sub> samples, factors related to primary emissions or secondary  
433 formation were identified. Opposite, performing the analysis on size-segregated samples led to the  
434 identification of local and regional factors. Indeed, running the model on size-segregated samples  
435 allowed ascribing part of the secondary compounds to local factors (e.g. traffic 1 and 2, wood  
436 burning) probably due to rapid formation of secondary particles in smaller size classes than  
437 secondary particles in regional (aged) aerosol. The regional aerosol factor was characterised by a  
438 high presence of secondary compounds, but not-negligible contributions primary source tracers (e.g.  
439 Cu, Fe, levoglucosan) were also present. The regional aerosol factor prevailed in the droplet mode,  
440 whereas the overall contribution from the two traffic sources dominated in the other size fractions.  
441 Further insights into the size-segregated profile suggested that the traffic 1 factor could be likely  
442 associated to diesel vehicles and the traffic 2 to gasoline vehicles.

443 It is noteworthy that 3-D source apportionment studies on aerosol separated in a number of size  
444 classes are nearly absent in the literature. The study presented here showed the possibility to apply  
445 3-D source apportionment studies to samples collected with multistage cascade impactors. Such  
446 samples can be analysed with traditional techniques (opposite to high-time resolved samples, which  
447 usually require to be analysed at accelerator facilities) and do not need dedicated instrumentation  
448 other than the sampler. In perspective, these features open the way to more frequent space-  
449 distributed size-segregated source apportionment studies, which are of primary importance to

450 optimise the effectiveness of future abatement strategies and to improve Earth radiation balance  
451 models.

452

### 453 **Acknowledgements**

454 This study was partially funded by the INFN experiment MANIA (Metodologie Analitiche  
455 Nucleari per Indagini Ambientali - Nuclear Analytical Methodologies for Environmental Research).

456 The authors are grateful to prof. Willy Maenhaut for MICRON tutorial and for providing mode  
457 interpolation program.

458 The authors are grateful to F. Cavaliere and D. Viganò of the Mechanical Workshop of the Physics  
459 Department for technical support.



461 **References**

- 462 Amato, F., Viana, M., Richard, A., Furger, M., Prévôt, A. S. H., Nava, S., Lucarelli, F.,  
463 Bukowiecki, N., Alastuey, A., Reche, C., Moreno, T., Pandolfi, M., Pey, J., and Querol, X. (2011).  
464 Size and time-resolved roadside enrichment of atmospheric particulate pollutants. *Atmospheric*  
465 *Chemistry and Physics*, 11, 2917-2931
- 466
- 467 Amato, F., Alastuey, A., Karanasiou, A., Lucarelli, F., Nava, S., Calzolari, Escrig A., Monfort E.,  
468 Sanfelix V., Gianelle V.L., Colombi C., Alves, C., Custódio, D., Nunes, T., Cerqueira, M., Pio, C.,  
469 Eleftheriadis, K., Diapouli, E., Reche, C., Minguillón, M. C., Manousakas, M.-I., Maggos, T.,  
470 Vratolis, S., Harrison, R. M., and Querol, X. (2016). Non-exhaust contributions to PM levels in 5  
471 EU cities. 10<sup>th</sup> International Conference on Air Quality - Science and Application, Milan, Italy, 14-  
472 18 March 2016. <https://drive.google.com/drive/folders/0B2iFZ3L-H5pRbGN4Q2NaeGNmQU0>
- 473
- 474 Belis, C.A., Larsen, B.R., Amato, F., El Haddad, I., Favez, O., Harrison, R.M., Hopke, P.K., Nava,  
475 S., Paatero, P., Prévôt, A., Quass, U., Vecchi, R., and Viana, M. (2014). European Guide on Air  
476 Pollution Source Identification with Receptor Models. EUR 26080 – Joint Research Centre –  
477 Institute for Environment and Sustainability. Luxembourg: Publications Office of the European  
478 Union.
- 479
- 480 Bernardoni, V., Cuccia, E., Calzolari, G., Chiari, M., Lucarelli, F., Massabò, D., Nava, S., Prati, P.,  
481 Valli, G., and Vecchi, R. (2011a). ED-XRF set-up for size-segregated aerosol samples analysis. *X-*  
482 *Ray Spectrometry*, 40, 79-87
- 483
- 484 Bernardoni, V., Vecchi, R., Valli, G. Piazzalunga, A., and Fermo, P. (2011b). PM10 source  
485 apportionment in Milan (Italy) using time-resolved data. *The Science of the Total Environment*,  
486 409, 4788-4795
- 487
- 488 Bonazza, A., Sabbioni, C., and Ghedini, N. (2005). Quantitative data on carbon fractions in  
489 interpretation of black crusts and soiling on European built heritage. *Atmospheric Environment*, 39,  
490 2607-2618
- 491
- 492 Bukowiecki, N., Hill, M., Gehrig, R., Lienemann, P., Zwicky, C. N., Hegedüs, F., Falkenberg, G.,  
493 Weingartner, E., and Baltensperger, U. (2005). Trace metals in ambient air: hourly size segregated  
494 mass concentrations determined by synchrotron-XRF. *Environmental Science and Technology*, 39,  
495 5754–5762

496  
497 Cabada, J.C., Rees, S., Takahama, S., Khlystov, A., Pandis, S.N., Davidson, C.I., and Robinson,  
498 A.L. (2004). Mass size distributions and size resolved chemical composition of fine particulate  
499 matter at the Pittsburgh supersite. *Atmospheric Environment*, 38, 3127-3141  
500  
501 Cahill, T.A. (1996). Climate Forcing by Anthropogenic Aerosols: The Role for PIXE. *Nuclear*  
502 *Instruments and Methods in Physics Research B: Beam Interactions with Materials and Atoms*,  
503 109/110, 402-406  
504  
505 Chandrasekaran, S.R., Laing, J.R., Holsen, T.M., Raja, S., and Hopke, P.K. (2011). Emission  
506 Characterization and Efficiency Measurements of High-Efficiency Wood Boilers. *Energy Fuels*, 25,  
507 5015–5021  
508  
509 Corsini, E., Vecchi, R., Marabini, L., Fermo, P., Becagli, S., Bernardoni, V., Caruso, D., Corbella,  
510 L., Dell'Acqua, M., Galli, C.L., Lonati, G., Ozgen, S., Papale, A., Signorini, S., Tardivo, R., Valli,  
511 G., and Marinovich, M. (2017). The chemical composition of ultrafine particles and associated  
512 biological effects at an alpine town impacted by wood burning. *Science of the Total Environment*,  
513 587-588, 223-231  
514  
515 Crilley, L.R., Lucarelli, F., Bloss, W.J., Harrison, R.M., Beddows, D.C., Calzolari, G., Nava, S.,  
516 Valli, G., Bernardoni, V., and Vecchi, R. (2017). Source apportionment of fine and coarse particles  
517 at a roadside and urban background site in London during the 2012 summer ClearfLo campaign.  
518 *Environmental Pollution*, 220, 766-778  
519  
520 EPA (2014). EPA Positive Matrix Factorization (PMF) 5.0 Fundamentals and User Guide.  
521 EPA/600/R-14/108, April 2014. [https://www.epa.gov/sites/production/files/2015-](https://www.epa.gov/sites/production/files/2015-02/documents/pmf_5.0_user_guide.pdf)  
522 [02/documents/pmf\\_5.0\\_user\\_guide.pdf](https://www.epa.gov/sites/production/files/2015-02/documents/pmf_5.0_user_guide.pdf)  
523  
524 Harshman, R. A. and Lundy, M. E. (1994). PARAFAC – Parallel Factor-Analysis. *Computational*  
525 *Statistics & Data Analysis*, 18, 39–72  
526  
527 Heal, M.R., Kumar, P., and Harrison, R.M. (2012). Particles, air quality, policy and health.  
528 *Chemical Society Reviews*, 41, 6606-6630  
529

530 Hillamo, R. E. (1994) Development of inertial impactor size spectroscopy for atmospheric aerosols.  
531 Ph.D. thesis  
532

533 Hopke, P.K. (2016). Review of receptor modeling methods for source apportionment. *Journal of the*  
534 *Air & Waste Management Association*, 66, 237-259  
535

536 Iinuma, Y., Brüggemann E., Gnauk T., Müller K., Andreae M. O., Helas G., Parmar R., and  
537 Herrmann H. (2007). Source characterization of biomass burning particles: The combustion of  
538 selected European conifers, African hardwood, savanna grass, and German and Indonesian peat.  
539 *Journal of Geophysical Research*, 112, D08209  
540

541 IPCC (2013). *Climate Change 2013: The Physical Science Basis. Contribution of Working Group I*  
542 *to the Fifth Assessment Report of the Intergovernmental Panel on Climate Change* [Stocker, T.F.,  
543 D. Qin, G.-K. Plattner, M. Tignor, S.K. Allen, J. Boschung, A. Nauels, Y. Xia, V. Bex and P.M.  
544 Midgley(eds.)]. Cambridge University Press, Cambridge, United Kingdom and New York, NY,  
545 USA, 1535 pp  
546

547 Kleeman, M.J., Schauer, J. J., and Cass, G. R. (1999). Size and Composition Distribution of Fine  
548 Particulate Matter Emitted from Wood Burning, Meat Charbroiling, and cigarettes. *Environmental*  
549 *Science and Technology*, 33, 3516-3523  
550

551 Li, N., Hopke, P.K., Kumar, P., Cliff, S.S., Zhao, Y., and Navasca, C. (2013). Source  
552 apportionment of time- and size-resolved ambient particulate matter. *Chemometrics and Intelligent*  
553 *Laboratory Systems*, 129, 15–20  
554

555 Lin, C.-C., Chen, S.-J., Huang, K.-L., Hwang, W.-I., Chang-Chien, G.-P., and Lin, W.-Y. (2005).  
556 Characteristics of metals in nano/ultrafine/fine/coarse particles collected beside a heavily Trafficked  
557 road. *Environmental Science and Technology*, 39, 8113–8122  
558

559 Link, M.F., Kim, J., Park, G., Lee, T., Park, T., Bin Babar, Z., Sung, K., Kim, P., Kang, S., Soo  
560 Kim, J., Choi, Y., Son, J., Lim, H.-J., and Farmer, D.K. (2017). Elevated production of NH<sub>4</sub>NO<sub>3</sub>  
561 from the photochemical processing of vehicle exhaust: Implications for air quality in the Seoul  
562 Metropolitan Region. *Atmospheric Environment*, 156, 95-101  
563

564 Maenhaut, W., Hillamo, R., Mäkelä, T., Jaffrezo, J.-L., Bergin, M.H., and Davidson, C.I. (1996). A

565 new cascade impactor for aerosol sampling with subsequent PIXE analysis. *Nuclear Instruments*  
566 *and Methods in Physics Research Section B: Beam Interactions with Materials and Atoms*, 109-  
567 110, 482-487  
568

569 Maenhaut, W., Jaffrezo, J.-L., Hillamo, R.E, Mäkelä, T, and Kerminen, V.-M. (1999). Size-  
570 fractionated aerosol composition during an intensive 1997 summer field campaign in northern  
571 Finland. *Nuclear Instruments and Methods in Physics Research Section B: Beam Interactions with*  
572 *Materials and Atoms*, 150, 345-349  
573

574 Maenhaut, W., Cafmeyer, J., Dubtsov, S., and Chi, X. (2002). Detailed mass size distributions of  
575 elements and species, and aerosol chemical mass closure during fall 1999 at Gent, Belgium.  
576 *Nuclear Instruments and Methods in Physics Research Section B: Beam Interactions with Materials*  
577 *and Atoms*, 189, 238-242  
578

579 Marcazzan, G.M., Ceriani M., Valli G., and Vecchi R. (2003). Source apportionment of PM10 and  
580 PM2.5 in Milan (Italy) using receptor modelling. *Science of the Total Environment*, 317, 137-147  
581

582 May, A., Nguyen, N., Presto, A., Gordon, T., Lipsky, E., Karve, M., Gutierrez, A., Robertson, W.,  
583 Zhang, M., Brandow, C., Chang, O., Chen, S., Cicero-Fernandez, P., Dinkins, L., Fuentes, M.,  
584 Huang, S., Ling, R., Long, J., Maddox, C., Massetti, J., McCauley, E., Miguel, A., Na, K., Ong, R.,  
585 Pang, Y., Rieger, P., Sax, T., Truong, T., Vo, T., Chattopadhyay, S., Maldonado, H., Maricq, M.,  
586 and Robinson, A. (2014). Gas- and particle-phase primary emissions from in-use, on-road gasoline  
587 and diesel vehicles. *Atmospheric Environment*, 88, 247-260  
588

589 Ozgen, S., Becagli, S., Bernardoni, V., Caserini, S., Caruso, D., Corbella, L., Dell'Acqua, M.,  
590 Fermo, P., Gonzalez, R., Lonati, G., Signorini, S., Tardivo, R., Tosi, E., Valli, G., Vecchi, R., and  
591 Marinovich, R. (2017). Analysis of the chemical composition of ultrafine particles from two  
592 domestic solid biomass fired room heaters under simulated real-world use. *Atmospheric*  
593 *Environment* 150, 87-97  
594

595 Paatero, P. (1999). The multilinear engine — a table-driven least squares program for solving  
596 multilinear problems, including the n-way parallel factor analysis model. *Journal of Computational*  
597 *and Graphical Statistics*, 8:4, 854-888  
598

599 Paatero, P. (2000). User's Guide for the Multilinear Engine Program "ME-2" for Fitting Multilinear

600 and Quasi-Multilinear Models. University of Helsinki: Helsinki, Finland  
601  
602 Paatero, P. (2015). User's Guide for Positive Matrix Factorization Programs PMF2 and PMF3, Part  
603 1–2: Tutorial. University of Helsinki: Helsinki, Finland (update 31 March 2015)  
604  
605 Pakkanen, T.A., Kerminen, V.-M. K., Korhonen, C.H., Hillamo, R.H., Aarnio, P., Koskentalo, T.,  
606 and Maenhaut, W. (2001). Use of atmospheric elemental size distributions in estimating aerosol  
607 sources in the Helsinki area. *Atmospheric Environment*, 39, 5363-5374  
608  
609 Pant, P., and Harrison, R.M. (2013). Estimation of the contribution of road traffic emissions to  
610 particulate matter concentrations from field measurements: A review. *Atmospheric Environment*,  
611 77, 78-97  
612  
613 Peré-Trepat, E., Kim, E., Paatero, P., and Hopke, P.K. (2007). Source apportionment of time and  
614 size resolved ambient particulate matter measured with a rotating DRUM impactor. *Atmospheric*  
615 *Environment*, 41, 5921–5933  
616  
617 Piazzalunga, A., Fermo, P., Bernardoni, V., Vecchi, R., Valli, G., and De Gregorio, M.A. (2010). A  
618 simplified method for levoglucosan quantification in wintertime atmospheric particulate matter by  
619 high performance anion-exchange chromatography coupled with pulsed amperometric detection.  
620 *International Journal of Environmental Analytical Chemistry*, 90, 934–947.  
621  
622 Piazzalunga, A., Bernardoni, V., Fermo, P., and Vecchi, R. (2013). Optimisation of analytical  
623 procedures for the quantification of ionic and carbonaceous fractions in the atmospheric aerosol and  
624 applications to ambient samples. *Analytical and Bioanalytical Chemistry*, 405, 1123- 1132  
625  
626 Pirjola, L., Niemi, J.V., Saarikoski, S., Aurela, M., Enroth, J., Carbone, S., Saarnio, K.,  
627 Kuuluvainen, H., Kousa, A., Rönkkö, T., and Hillamo, R. (2017). Physical and chemical  
628 characterization of urban winter-time aerosols by mobile measurements in Helsinki, Finland.  
629 *Atmospheric Environment*, 158, 60-75  
630  
631 Polissar, A.V., Hopke, P.K., Paatero, P., Malm, W.C., and Sisler, J.F. (1998). Atmospheric aerosol  
632 over Alaska: 2. Elemental composition and sources. *Journal of Geophysical Research*, 103, 19045-  
633 19057  
634

635 Pope, C.A. III, and Dockery, D.W. (2006). Health Effects of Fine Particulate Air Pollution: Lines  
636 that Connect. *Journal of Air & Waste Management Association*, 56, 709-742  
637

638 Pöschl, U. (2005). Atmospheric Aerosols: Composition, Transformation, Climate and Health  
639 Effects. *Angewandte Chemie International Edition*, 44, 7520-7540  
640

641 Raabe, O.G., Braaten, D.A., Axelbaum, R.L., Teague, S., and Cahill, T. (1988). Calibration studies  
642 of the DRUM impactor. *Journal of Aerosol Science*, 19, 183-195  
643

644 Robert, M. A., Kleeman, M.J., and Jakober, C.A. (2007). Size and Composition Distributions of  
645 Particulate Matter Emissions: Part 2—Heavy-Duty Diesel Vehicles. *Journal of the Air & Waste  
646 Management Association*, 57, 1429-1438  
647

648 Rogula-Kozłowska, W. (2016). Size-segregated urban particulate matter: mass closure, chemical  
649 composition, and primary and secondary matter content. *Air Quality, Atmosphere and Health*, 9,  
650 533-550  
651

652 Salma, I., Ocskay, R., Raes, N., and Maenhaut, W. (2005). Fine structure of mass size distributions  
653 in an urban environment. *Atmospheric Environment*, 39, 5363-5374  
654

655 Schauer, J.J., Lough G.C., Shafer M.M., Christensen W.F., Arndt M.F., DeMinter J.T., and Park, J.-  
656 S. (2006). Characterization of Metals Emitted from Motor Vehicles. Research Report 133. Health  
657 Effects Institute, Boston MA  
658

659 Seinfeld, J.H., and Pandis, S.N. (1998). *Atmospheric Chemistry and Physics from air pollution to  
660 climate change*. New York. John Wiley and Sons, Incorporated  
661

662 Simoneit, B.R.T., Schauer, J.J., Nolte, C.G., Oros, D.R., Elias, V.O., Fraser, M.P., Rogge, W.F.,  
663 and Cass, G.R. (1999). Levoglucosan, a tracer for cellulose in biomass burning and atmospheric  
664 particles. *Atmospheric Environment*, 33, 173-182.  
665

666 Tucker, L. R. (1966). Some Mathematical Notes on 3-Mode Factor Analysis. *Psychometrika*, 31,  
667 279–311  
668

669 Ulbrich, I. M., Canagaratna, M. R., Cubison, M. J., Zhang, Q., Ng, N. L., Aiken, A. C., and

670 Jimenez, J. L. (2012). Three-dimensional factorization of size-resolved organic aerosol mass spectra  
671 from Mexico City. *Atmospheric Measurement Techniques*, 5, 195-224.  
672

673 Vecchi R., Marcazzan G., Valli G., Ceriani M., and Antoniazzi C. (2004). The role of atmospheric  
674 dispersion in the seasonal variation of PM1 and PM2.5 concentration and composition in the urban  
675 area of Milan (Italy). *Atmospheric Environment*, 38, 4437-4446  
676

677 Vecchi R., Bernardoni V., Fermo P., Lucarelli F., Mazzei F., Nava S., Prati P., Piazzalunga A., and  
678 Valli G. (2009). 4-hours resolution data to study PM10 in a “hot spot” area in Europe.  
679 *Environmental Monitoring and Assessment*, 154, 283-300.  
680

681 Viana, M., Kuhlbusch, T.A.J., Querol, X., Alastuey, A., Harrison, R.M., Hopke, P.K., Winiwarter,  
682 W., Vallius, M., Szidat, S., Prévôt, A.S.H., Hueglin, C., Bloemen, H., Wählín, P., Vecchi, R.,  
683 Miranda, A.I., Kasper-Giebl, A., Maenhaut W., and Hitzenberger R. (2008). Source apportionment  
684 of particulate matter in Europe: A review of methods and results. *Journal of Aerosol Science* 39,  
685 827-849  
686

687 Viidanoja, J., Kerminen, V.-M., and Hillamo, R. (2002). Measuring the size distribution of  
688 atmospheric organic and black carbon using impactor sampling coupled with thermal carbon  
689 analysis: Method development and uncertainties. *Aerosol Science and Technology*, 36, 607-616.  
690

691 Wang Y., and Hopke P.K. (2013). A ten-year source apportionment study of ambient fine  
692 particulate matter in San Jose, California. *Atmospheric Pollution Research*, 4, 398-404  
693

694 Watson J.G. (2002). Visibility: Science and Regulation. *Journal of Air & Waste Management*  
695 *Association* 52, 628–713  
696

697 Wolfenbarger, J.K., and Seinfeld, J.H. (1990). Inversion of size distribution data. *Journal of Aerosol*  
698 *Science*, 21, 227-247

700 **Figure captions**

701 *Figure 1: example of modes reconstruction: a) histogram representation obtained from data*  
702 *measured on each impaction stage; b) data inversion by the program MICRON; c) modes*  
703 *interpolation. The example is referred to the mass size distribution of one of the collected samples.*

704

705 *Figure 2: average type 1 and type 2 mass size distributions*

706

707 *Figure 3: average size distribution for secondary ions (a), wood burning markers (b), traffic*  
708 *markers (c)*

709

710 *Figure 4: left panel: factor profiles (black bars) and percent species (grey dots); right panel: factor*  
711 *mass size distributions*

712

713 *Figure 5: histogram representation of the size-segregated relative contribution of the species to the*  
714 *identified factors. Normalisation was carried out to the total average concentration of each species.*  
715 *For each species, x-axis represents  $\log(d_p)$  and the x-axis scale is the same as histograms in figure*  
716 *1 and figure 4. Cut-off size for each represented stage (i.e. left-end of coloured bars) are reported*  
717 *in the legend.*

718

719 *Figure 6: mode-segregated source apportionment. Sum of percentages is  $100\% \pm 1\%$  due to number*  
720 *rounding.*

721

722 *Figure 7: histogram representation of size-segregated distribution of (a) Cu, (b) Mn, and (c) Zn in*  
723 *the traffic 1 and traffic 2 factors profile. Normalisation to the total concentration of the species to*  
724 *each factor profile was carried out. For each component, x-axis represents  $\log(d_p)$  and the x-axis*  
725 *scale is the same as histograms in figure 1 and figure 4. Cut-off size for each represented stage (i.e.*  
726 *left-end of coloured bars) are reported in the legend.*

727



728 *Table 1: geometric mean aerodynamic diameter (GMAD), relative mass concentration (RMC), and relative number of cases of mode presence (n.cases)*  
 729 *for Aitken, condensation, droplet, coarse modes and very large particles. RMC evaluation was limited to the cases in which the mode was present.*

	Aitken mode			Condensation mode			Droplet mode			Coarse mode			Very large particles		
	GMAD ( $\mu\text{m}$ )	RMC (%)	n. cases (%)	GMAD ( $\mu\text{m}$ )	RMC (%)	n. cases (%)	GMAD ( $\mu\text{m}$ )	RMC (%)	n. cases (%)	GMAD ( $\mu\text{m}$ )	RMC (%)	n. cases (%)	GMAD ( $\mu\text{m}$ )	RMC (%)	n. cases (%)
<b>S</b>				0.28	30%	86%	0.66	59%	100%	3.4	17%	71%			
<b>Cl</b>				0.36	18%	86%	0.72	29%	71%	4.4	61%	100%	16.1	10%	36%
<b>K</b>				0.26	31%	86%	0.58	46%	100%	3.7	25%	100%	15.7	9%	29%
<b>Ca</b>										3.9	79%	100%	15.7	11%	86%
<b>Ti</b>				0.22	5%	36%				3.5	71%	100%	15.1	13%	64%
<b>Cr</b>				0.31	17%	36%	0.67	38%	57%	2.9	64%	100%	4.7	29%	29%
<b>Mn</b>				0.30	13%	43%	0.72	42%	100%	3.2	50%	100%	15.7	10%	21%
<b>Fe</b>				0.42	6%	21%				3.2	74%	100%	16.6	7%	43%
<b>Ni</b>				0.28	21%	43%	0.48	45%	86%	3.0	50%	93%			
<b>Cu</b>				0.27	6%	71%				3.0	72%	100%	16.3	7%	21%
<b>Zn</b>				0.27	14%	79%	0.77	49%	93%	2.7	43%	100%	14.5	9%	14%
<b>Levogluosan</b>	0.10	4%	100%	0.32	56%	100%	0.63	43%	78%	1.6	5%	78%	5.2	3%	78%
<b>K<sup>+</sup></b>	0.10	4%	44%	0.29	49%	89%	0.62	37%	89%	1.9	4%	22%	4.1	12%	89%
<b>NO<sub>3</sub><sup>-</sup></b>	0.11	2%	100%	0.31	28%	100%	0.71	61%	100%	2.4	6%	67%	4.0	10%	56%
<b>SO<sub>4</sub><sup>=</sup></b>	0.10	4%	100%	0.29	31%	100%	0.67	52%	100%	1.69	8%	56%	4.5	10%	100%
<b>NH<sub>4</sub><sup>+</sup></b>	0.10	2%	89%	0.31	35%	100%	0.70	62%	100%	3.5	2%	44%	8.2	1%	67%

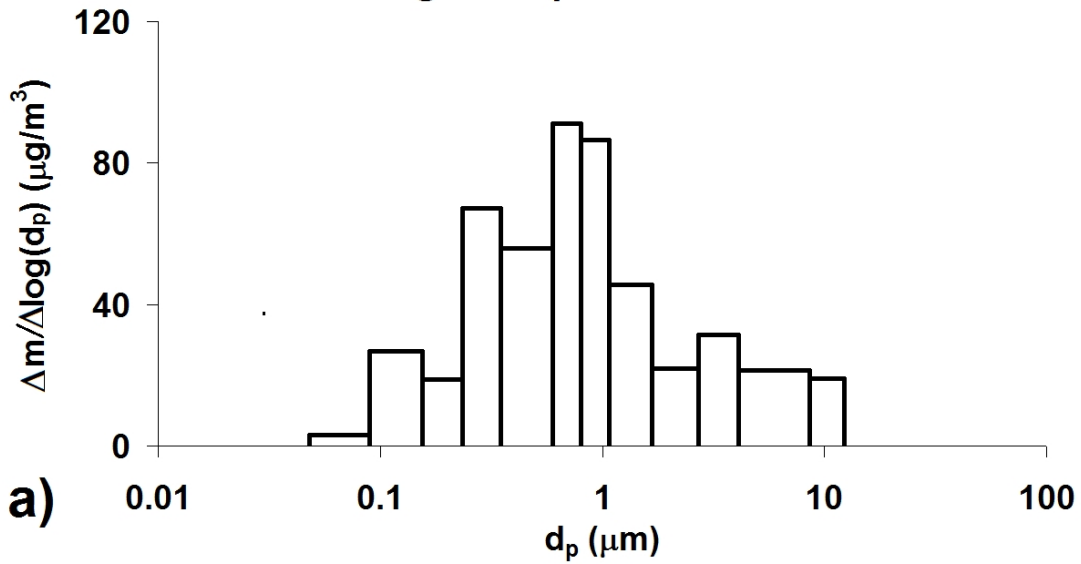
730

732 Table 2: geometric mean aerodynamic diameter (GMAD) and mode relative mass contribution (RMC) to each factor.

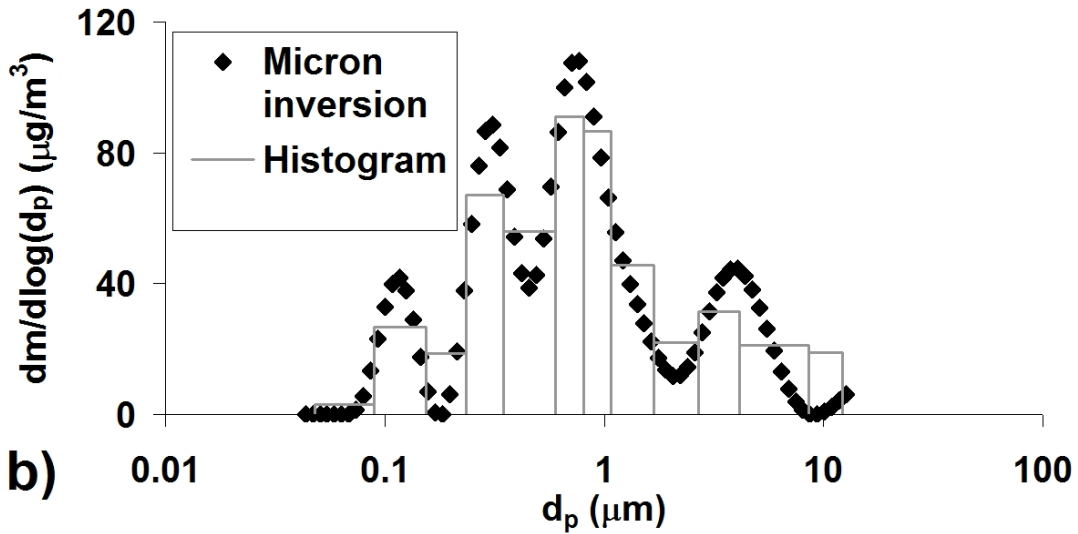
Factor name		Aitken mode	Condensation submode	Droplet submode	Coarse mode	Very large particles
Wood Burning	GMAD ( $\mu\text{m}$ )	0.036	0.210	0.599		
	Relative contribution	4%	24%	72%		
Industry	GMAD ( $\mu\text{m}$ )	0.105	0.298		1.31	6.39
	Relative contribution	6%	58%		17%	19%
Resuspended Dust	GMAD ( $\mu\text{m}$ )		0.292	0.586	2.99	9.15
	Relative contribution		33%	23%	34%	10%
Regional	GMAD ( $\mu\text{m}$ )		0.203	0.695	2.81	
	Relative contribution		9%	81%	10%	
Construction works	GMAD ( $\mu\text{m}$ )	0.034	0.189	0.567	2.61	7.53
	Relative contribution	11%	14%	25%	12%	37%
Traffic 1	GMAD ( $\mu\text{m}$ )	0.118	0.344	0.98	2.97	9.30
	Relative contribution	5%	28%	33%	23%	12%
Traffic 2	GMAD ( $\mu\text{m}$ )	0.094	0.286	0.823	4.18	
	Relative contribution	7%	31%	38%	24%	

733

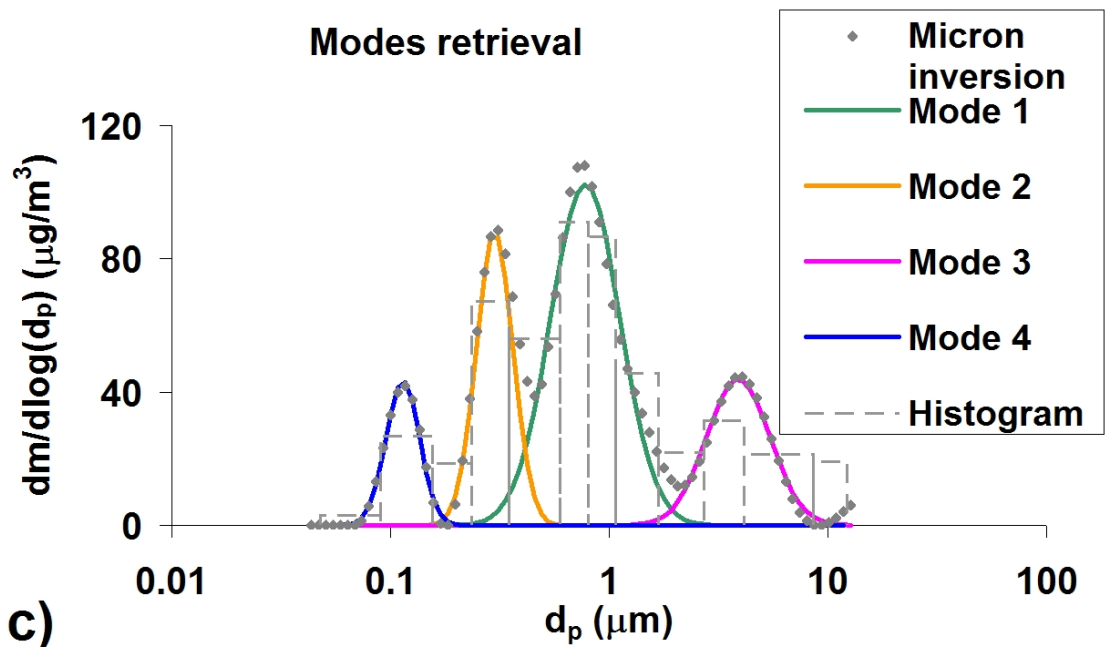
### Histogram representation



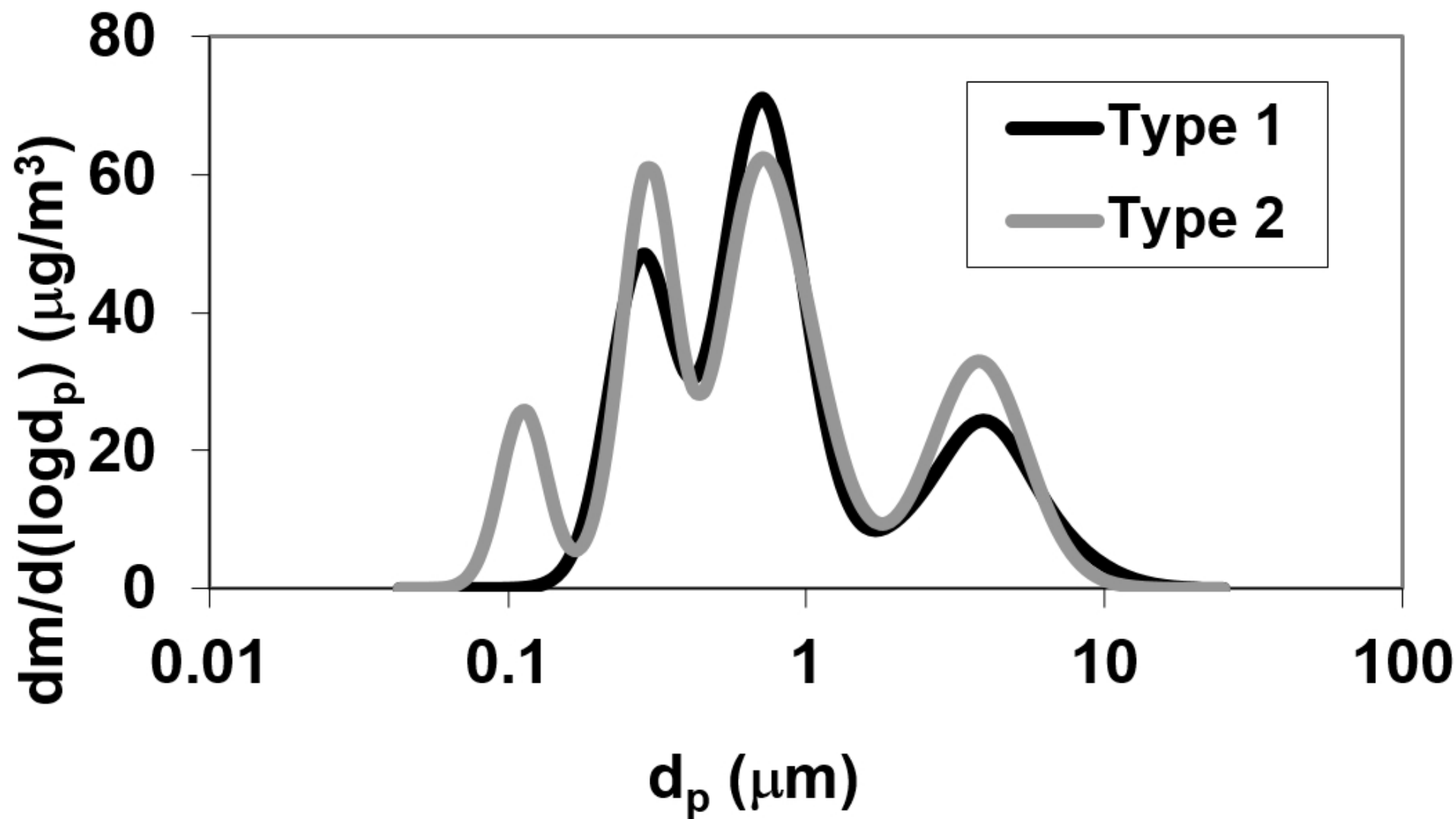
### Micron inversion



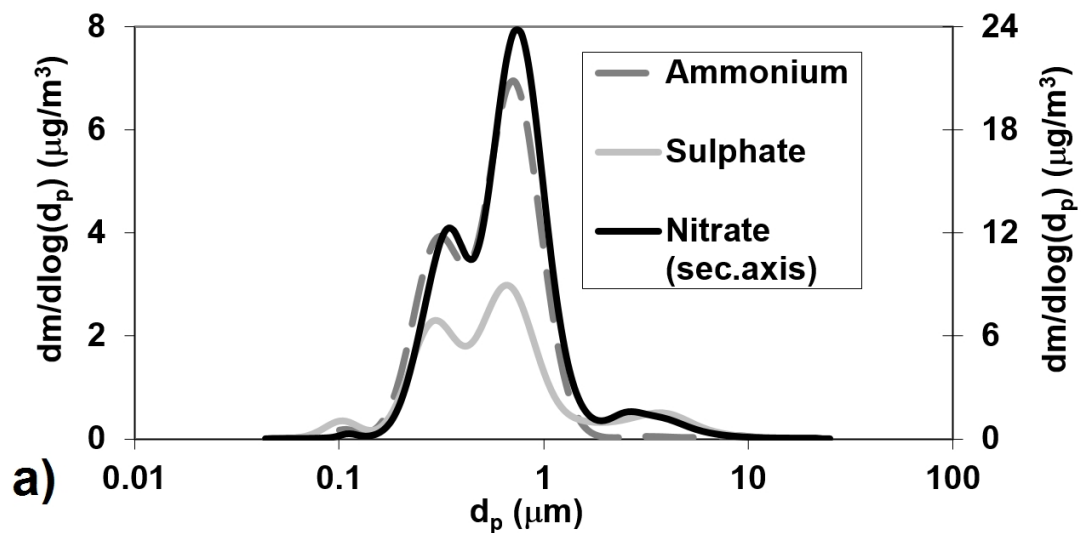
### Modes retrieval



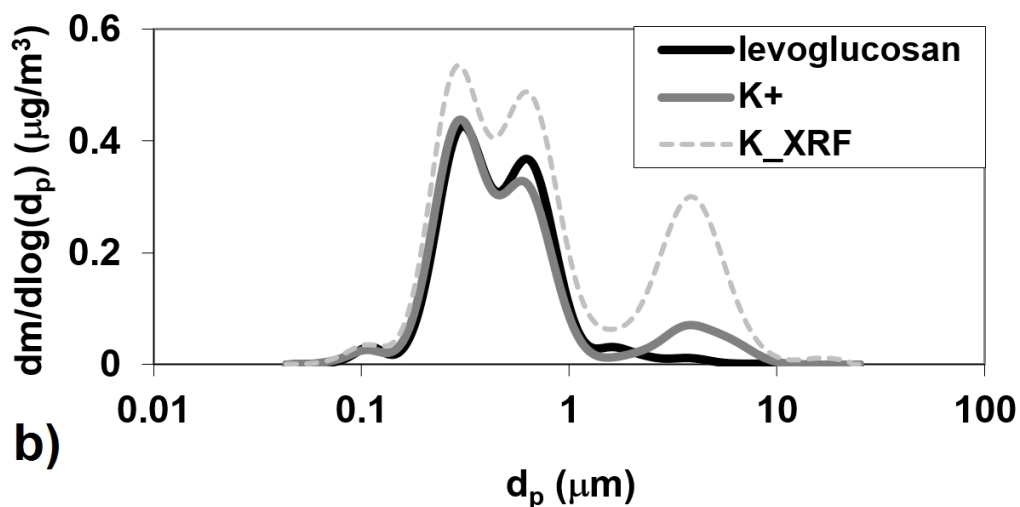
# Average mass size distribution



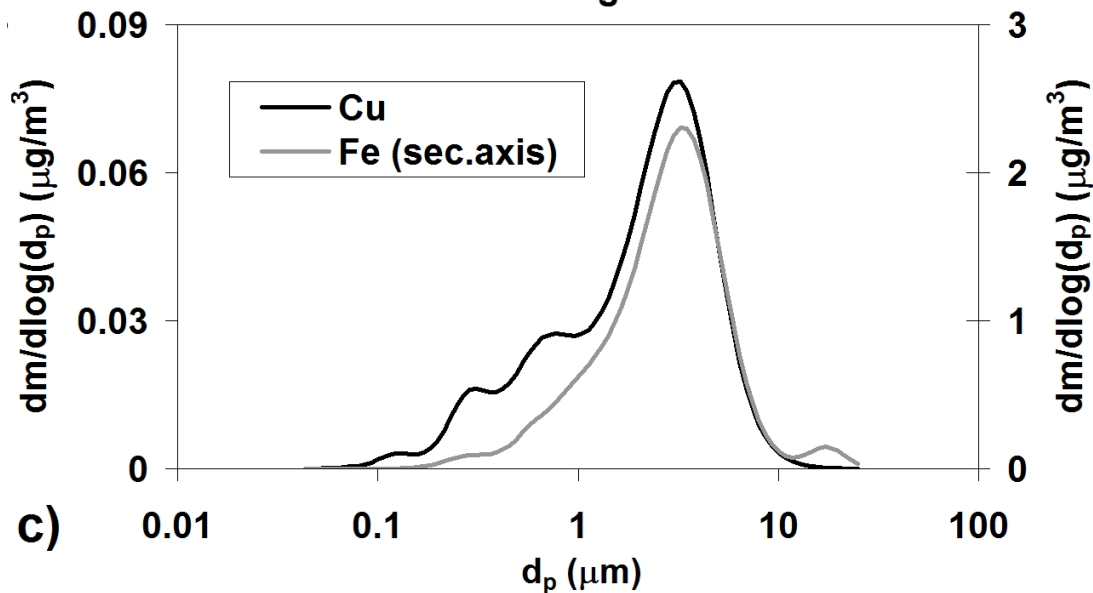
### Secondary inorganic ions: average size distribution

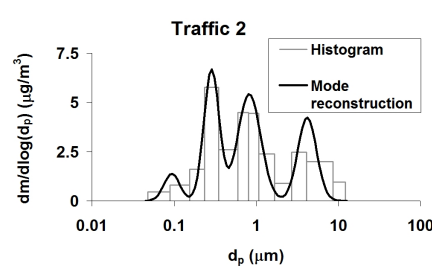
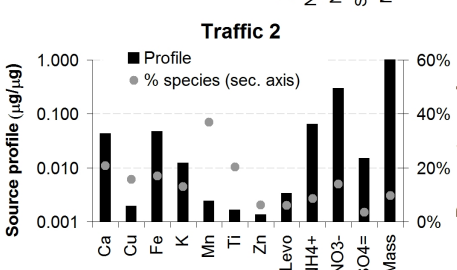
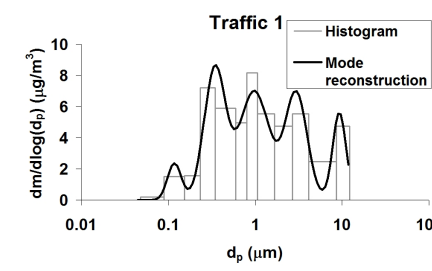
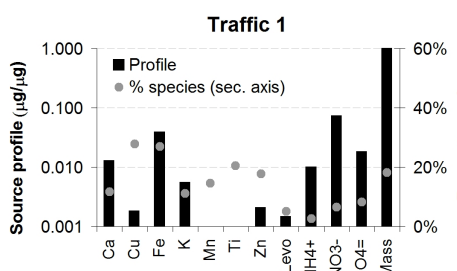
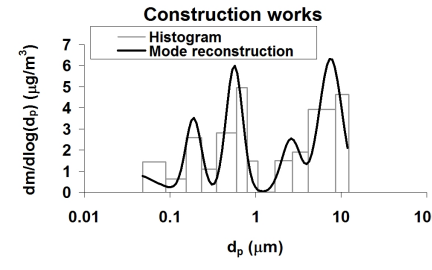
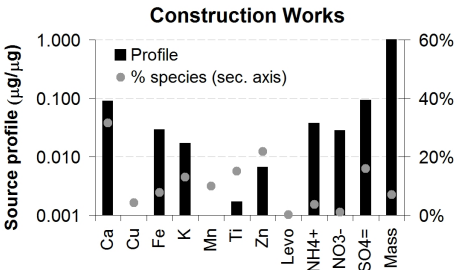
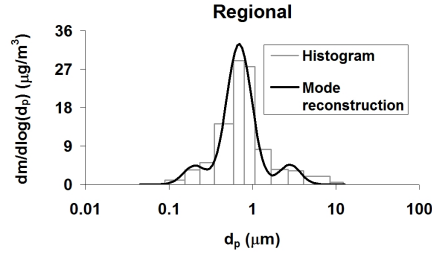
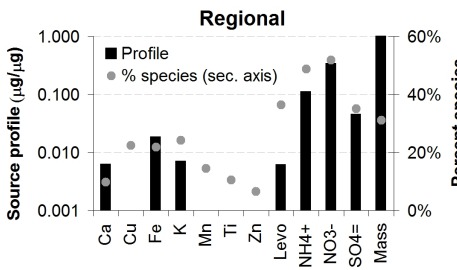
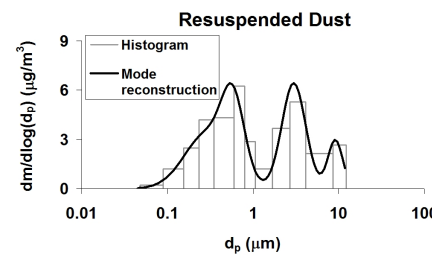
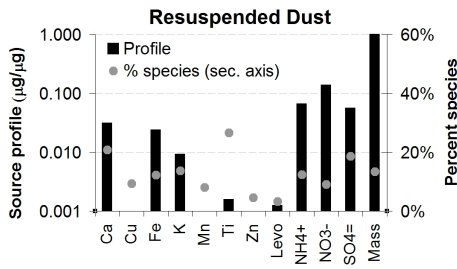
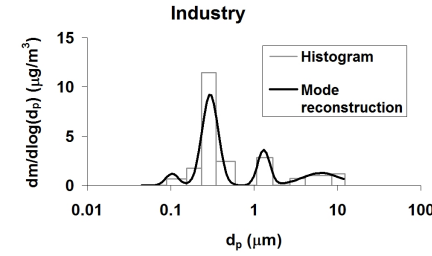
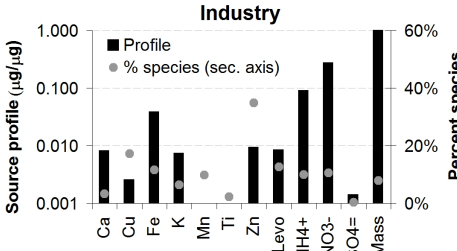
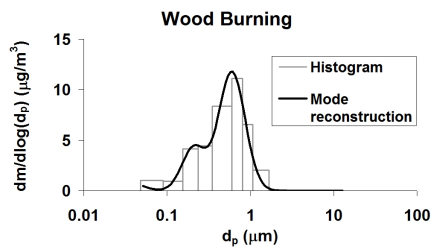
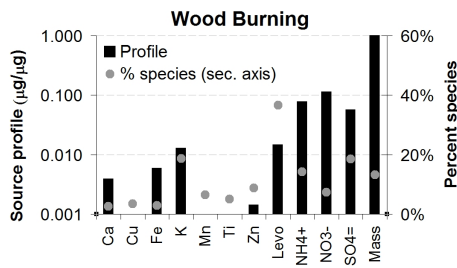


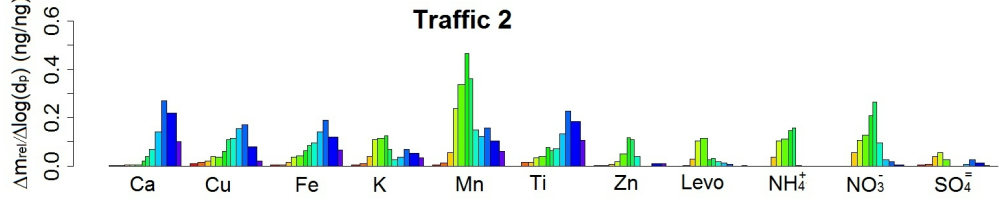
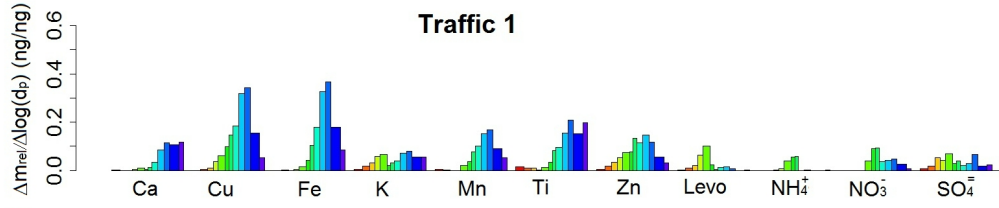
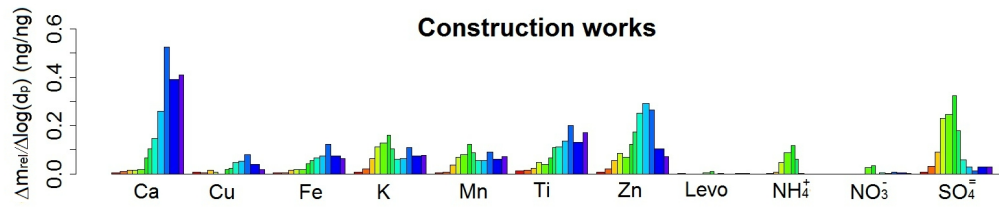
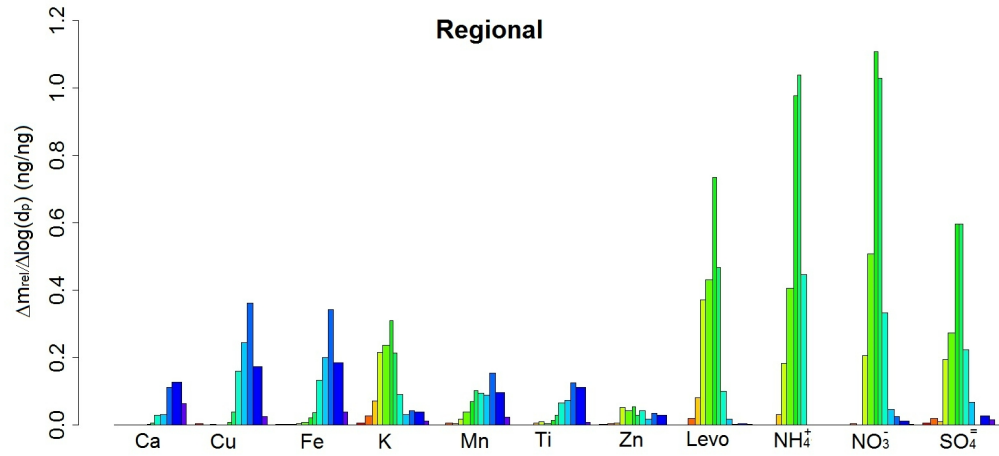
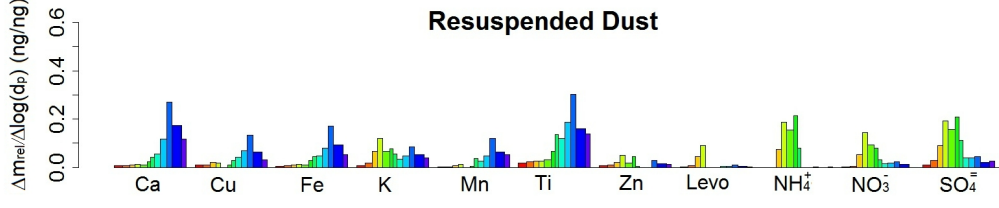
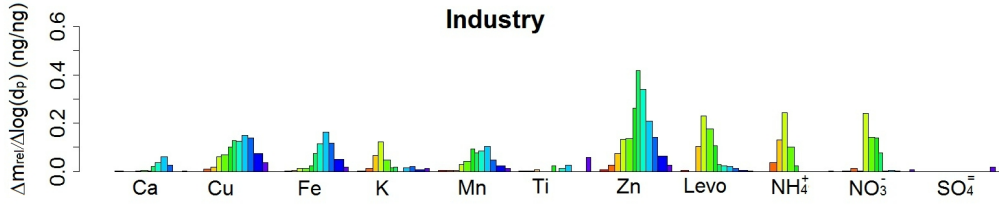
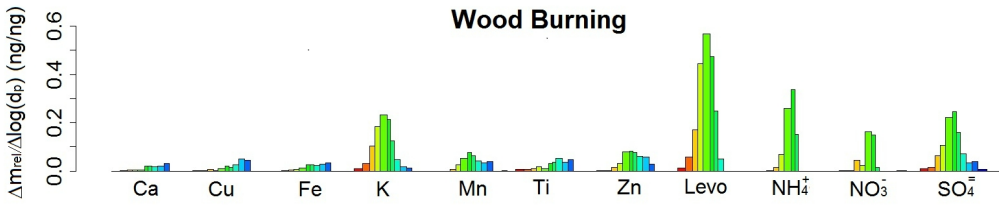
### Wood burning markers: average size distribution



### Traffic markers: average size distribution

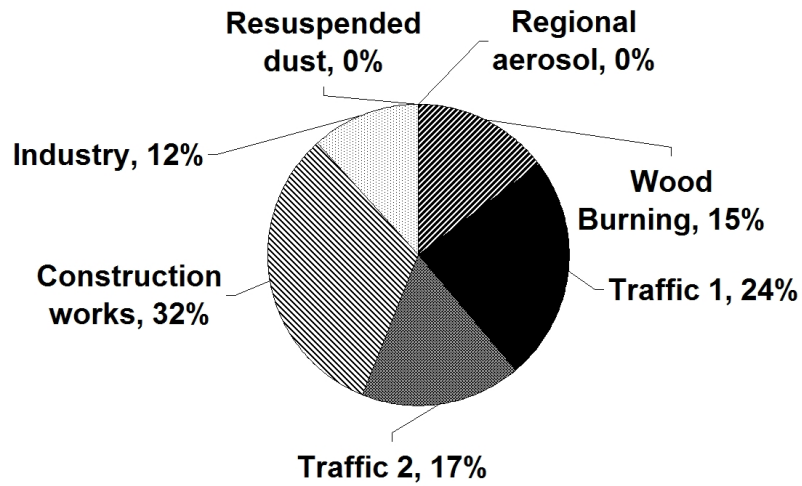




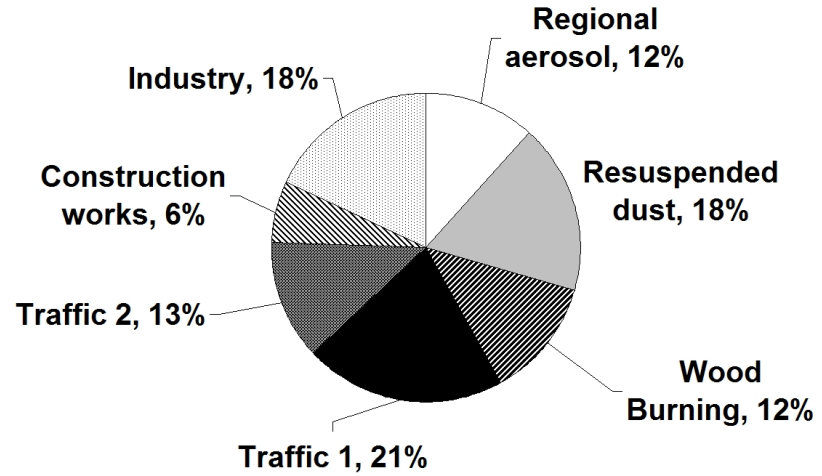


Cut-off diameter ( $\mu\text{m}$ )			
0.048	0.235	0.804	2.70
0.090	0.349	1.07	4.12
0.155	0.598	1.68	8.57

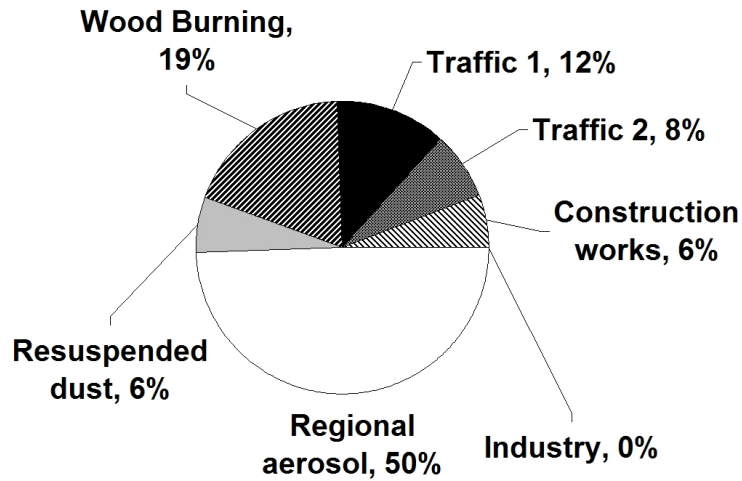
### AITKEN MODE



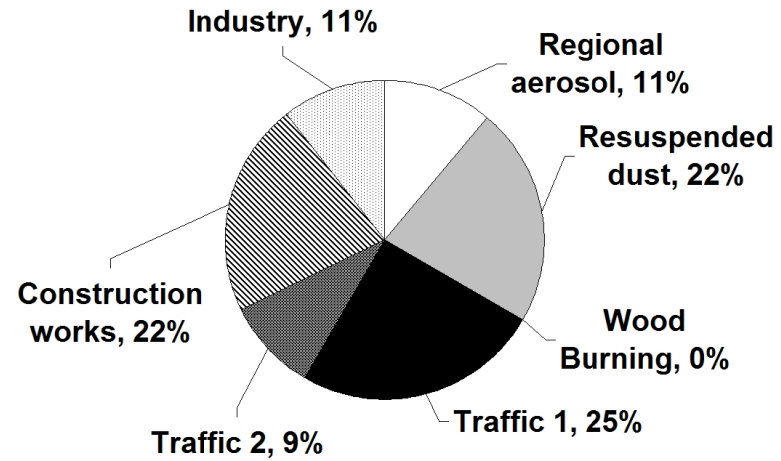
### CONDENSATION MODE



### DROPLET MODE

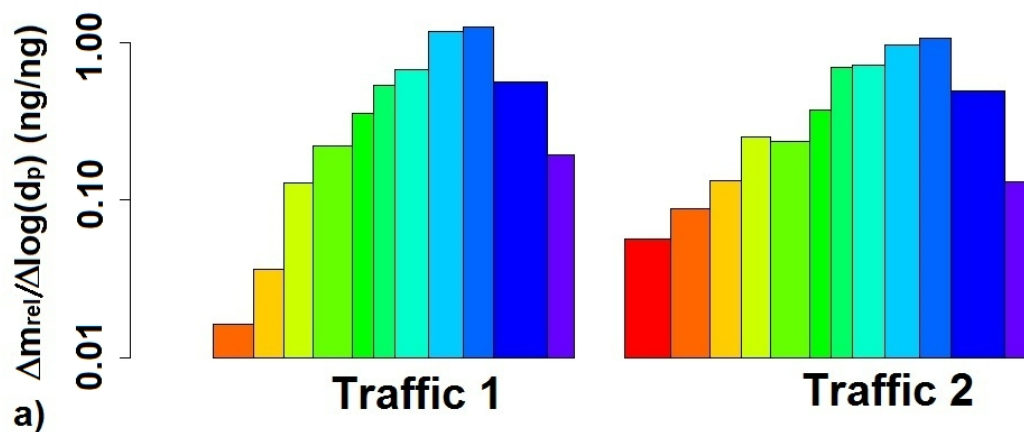


### COARSE MODE AND VERY LARGE PARTICLES





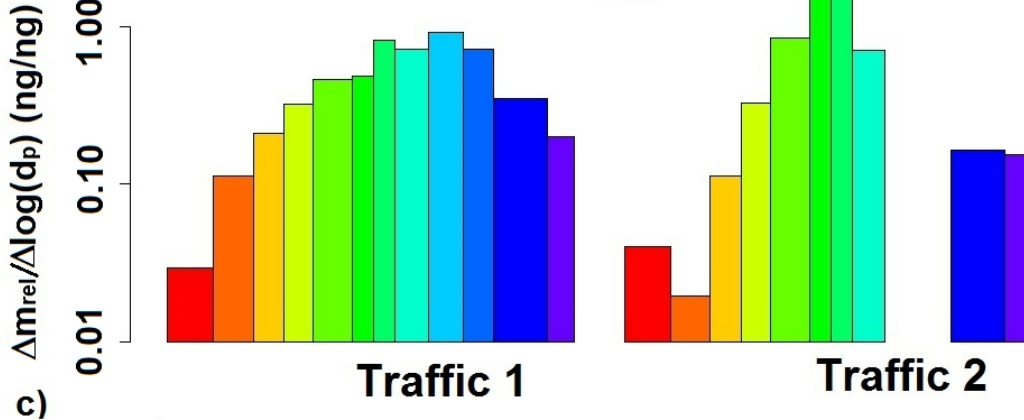
**Cu**



**Mn**



**Zn**



**Cut-off diameter ( $\mu\text{m}$ )**

0.048	0.235	0.804	2.70
0.090	0.349	1.07	4.12
0.155	0.598	1.68	8.57